Structural Engineering and Mechanics, *Vol. 73, No. 3 (2020) 353-365*
DOI: https://doi.org/10.12989/sem.2020.73.3.353

Timber-FRP composite beam subjected to negative bending

Mahbube Subhani*[1], Anastasia Globa[2a] and Jules Moloney[3b]

[1]*School of Engineering, Deakin University, Waurn Ponds, VIC 3216, Australia*
[2]*School of Architecture, Design and Planning, University of Sydney, NSW 2008, Australia*
[3]*School of Design, RMIT University, Melbourne 3001, Australia*

(Received February 28, 2019, Revised May 7, 2019, Accepted October 13, 2019)

Abstract. In the previous studies, the authors proposed the use of laminated veneer lumber – carbon fiber reinforced polymer (LVL-CFRP) composite beams for structural application. Bond strength of the LVL-to-CFRP interface and flexural strengthening schemes to increase the bending capacity subjected to positive and negative moment were discussed in the previous works. In this article, theoretical models are proposed to predict the moment capacity when the LVL-CFRP beams are subjected to negative moment. Two common failure modes – CFRP fracture and debonding of CFRP are considered. The non-linear model proposed for positive moment is modified for negative moment to determine the section moment capacity. For the debonding based failure, previously developed bond strength model for CFRP-to-LVL interface is implemented. The theoretical models are validated against the experimental results and then use to determine the moment-rotation behaviour and rotational rigidity to compare the efficacy of various strengthening techniques. It is found that combined use of bi- and uni-directional CFRP U-wrap at the joint performs well in terms of both moment capacity and rotational rigidity.

Keywords: CFRP, LVL; negative moment; composites; analytical modelling; moment-rotation

1. Introduction

With the advancement of engineering wood products, such as laminated veneer lumber (LVL), glue laminated timber (glulam) and cross-laminated timber (CLT), mid-rise construction of timber building is gaining attention. However, design and construction of mid-rise timber structures is experiencing new challenges. For mid-rise construction, long span beams require higher moment capacity. To overcome this limitation, different techniques, such as, use of densified veneer wood (Guan and Rodd 2003), steel plates (Biscaia *et al*. 2017) and light weight and high strength materials, such as fibre reinforced polymer (FRP) were reported. Various FRP materials, such as glass FRP (Raftery and Harte 2011, Alhayek and Svecova 2012, Fossetti *et al*. 2015), carbon FRP (Schober and Rautenstrauch 2005, Khelifa and Celzard 2014, Khelifa *et al*. 2015, Khelifa *et al*. 2015, Biscaia *et al*. 2016), basalt FRP (de la Rosa García *et al*. 2013, Fossetti *et al*. 2015, de la Rosa García *et al*. 2016) are reported to use in various forms which includes external FRP strips (Fiorelli and Dias 2003, Schober and Rautenstrauch 2005, Li *et al*. 2009, Khelifa *et al*. 2015, Khelifa *et al*. 2015), embedded rods (Micelli *et al*. 2005, Fossetti *et al*. 2015, Schober *et al*. 2015), pre-stressing (Miljanovic and Zlatar 2015), U-wraps (de la Rosa García *et al*. 2013, de la Rosa García *et al*. 2016) and embedded and external FRP plates (Raftery and Harte 2011, Juvandes and Barbosa 2012, Nowak *et al*. 2013, D'Ambrisi *et al*. 2014, Chun *et al*. 2016) to produce timber-FRP composite beams. However, all of these research focused mainly on the efficiency of the beams under positive moment.

The common failure modes observed for positive moment are debonding of FRP, FRP fracture and tensile rupture of timber. For the debonding based failure, there are a number of factors which affects the bond performance of timber-to-FRP interface. Various researchers consider different effects which influence the bond strength, such as, annual growth rings (Smith 2011), bond length, position of pith, adhesive and wooden species (Wan *et al*. 2011) and bond length, surface configuration and direction of glulam fibres (De Lorenzis *et al*. 2005). Juvendes and Barbosa (2012) also proposed an equation to consider the effects of some of these parameters. However, since FRP is a transversely isotropic material, the relative angle between the fibre orientation of FRP and grain orientation of timber also affect the interfacial bond strength of timber-FRP composites.

In one of the previous work (Subhani *et al*. 2017), the authors discussed the effect of the surface of LVL beam (grain and laminate face of LVL) on which CFRP are usually attached. In addition, the orientation of CFRP fibre with respect to LVL grain direction (parallel and perpendicular to each other) were also taken into account. Pull-out tests were performed to investigate these effects. The effect of these two parameters are included in the Juvendes and Barbosa model (2012) which found to be accurate in terms of predicting bond strength and can be

*Corresponding author, Ph.D.
E-mail: mahbube.subhani@deakin.edu.au
[a] Ph.D.
E-mail: anastasia.globa@sydney.edu.au
b Ph.D.
E-mail: jules.moloney@rmit.edu.au

http://www.techno-press.com/journals/sem&subpage=7
ISSN: 1225-4568 (Print), 1598-6217 (Online)

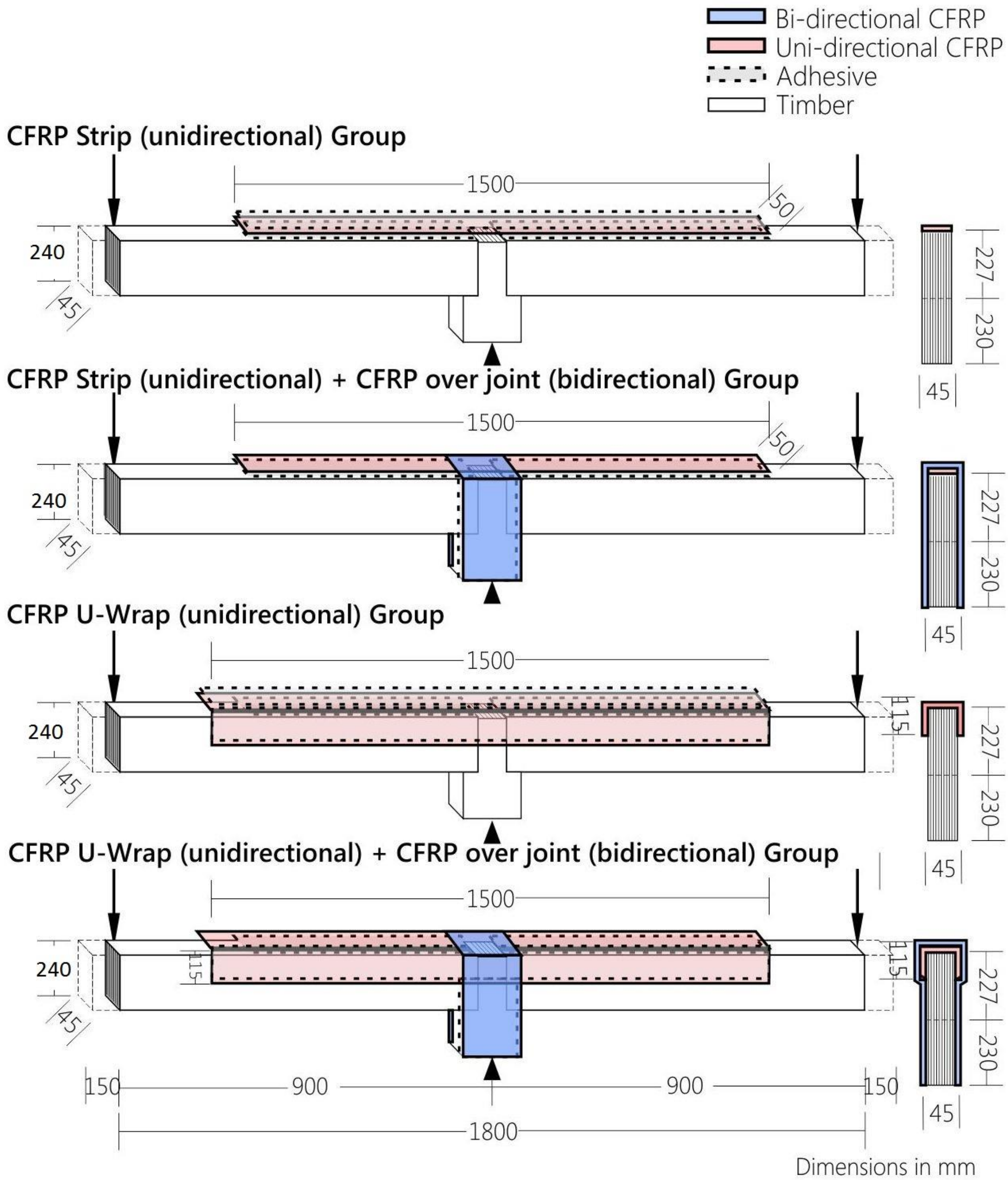

Fig. 1 Four strengthening techniques for negative bending moment (after (Globa *et al*. 2018)

considered for debonding based failure of LVL-CFRP composite beams.

Following the previous work on the bond strength, the authors proposed theoretical model to predict the moment capacity of LVL-CFRP composite beams subjected to positive moment (Subhani *et al*. 2017). It was concluded that non-liner model yield slightly more accurate prediction in terms moment capacity. Then the strengthening schemes used for positive moments along with two additional ones were implemented for negative moment by the authors in (Globa *et al*. 2018).

In the present study, previously developed non-linear model is used to predict the negative moment carrying capacity of the LVL-CFRP composite beams. Both CFRP fracture and debonding based failure are considered for the theoretical development. The aforementioned effect of LVL surface and LVL-to-CFRP orientation are considered in the debonding based model of the composite beam under bending. Additionally, the moment-rotation behaviour of the composite beam subjected to both positive and negative moments is determined from the theoretical model and compared. Lastly, the rotational rigidity of different strengthening techniques is calculated to conclude which scheme is most effective to provide continuity of the LVL beams at the beam-column joint.

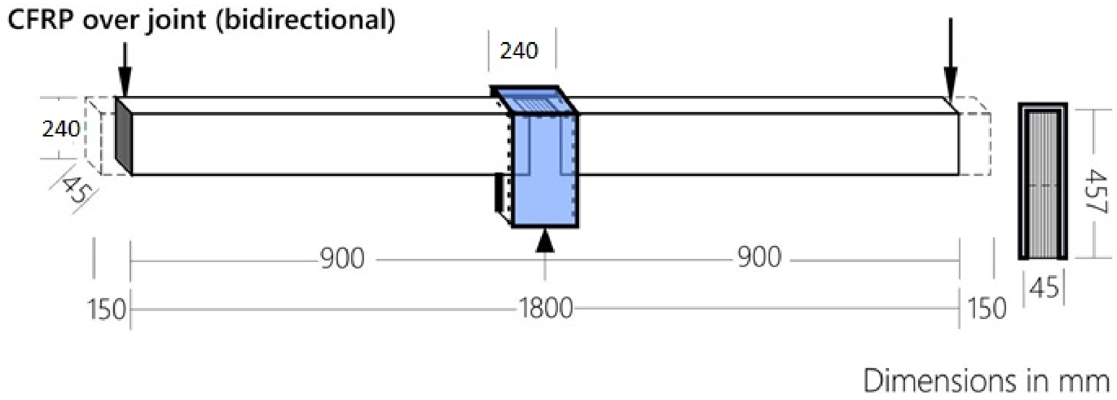

Fig. 2 Strengthening for negative bending moment capacity of composite beam using bi-directional CFRP

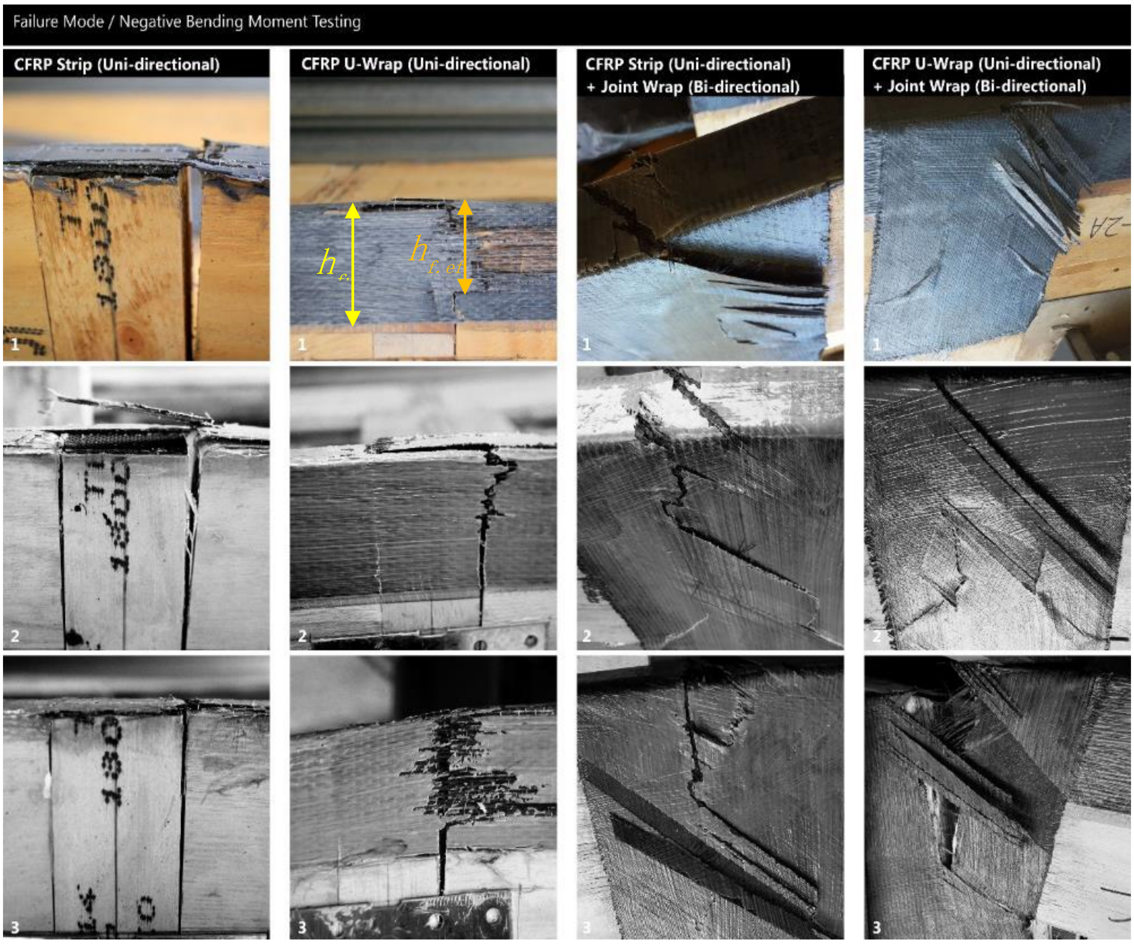

Fig. 3 Failure modes of Scheme 1, 2, 4 and 5 (after (Globa *et al*. 2018))

2. Strengthening Schemes

The In the previous work (Globa *et al*. 2018) by the authors, five types of strengthening techniques were proposed for negative moment bending testing, as shown in Fig. 1. Two LVL beams and one LVL column piece were connected using uni- directional and/or bi-directional CFRP to provide structural continuity of LVL beams. These four schemes were

- Scheme 1: Uni-directional CFRP Strip
- Scheme 2: Uni-directional CFRP U-wrap
- Scheme 4: Combination of uni-directional CFRP Strip and joint wrap using bi-directional CFRP
- Scheme 5: Combination of uni-directional CFRP U-wrap and joint wrap using bi-directional CFRP

In addition to these four Schemes, one additional testing were conducted with the following combination

- Scheme 3: Joint wrap with bi-directional CFRP (Fig. 2) [one sample]

The detail of the experimental program and analysis of the result can be found in (Globa *et al*. 2018). The failure

Fig. 4 Failure mode observed for Scheme 3

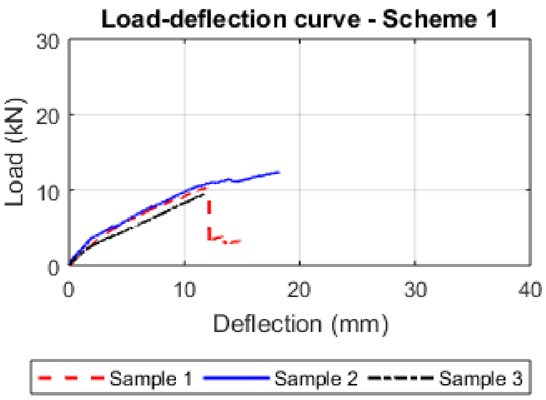

(a) Scheme 1

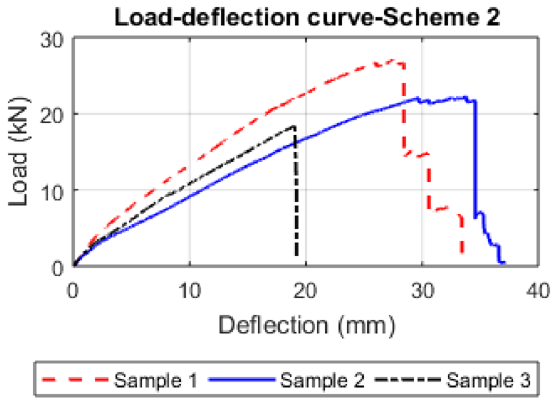

(b) Scheme 2

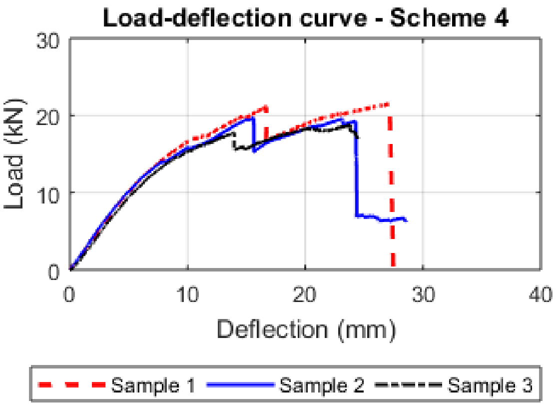

(c) Scheme 4

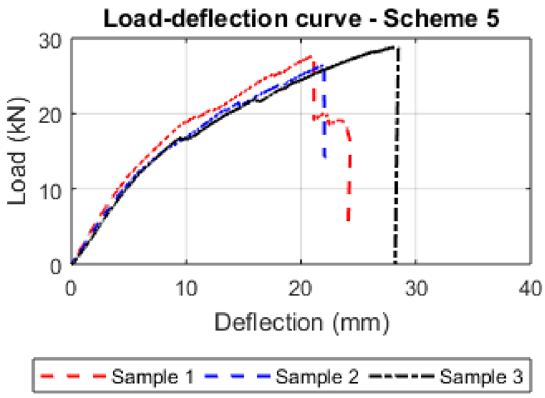

(d) Scheme 5

Fig. 5 Load-deflection curve of Scheme 1, 2, 4 and 5 (recreated from (Globa *et al*. 2018))

mode of Scheme 1, 2, 4 and 5 is illustrated in Fig. 3. Two types of failure modes were observed - CFRP fracture (Scheme 1 and 2) and delamination of bi-directional CFRP for Scheme 4 and 5. Fig. 4 depicts the failure mode of Scheme 3 which is initiated by the delamination of bi-directional CFRP.

For the completeness of this article, the load-deflection curves for Scheme 1, 2, 4 and 5 (reported in (Globa *et al.* 2018)) are recreated in Fig. 5. Also, the ultimate load for each samples associated with all the five strengthening schemes are tabulated in Table 1. It can be observed that the implementation of bi-directional CFRP yield consistent behaviour in terms of load-deflection curves and ultimate load carrying capacity. The most inconsistent results were obtained for Scheme 2 in terms of both load-deflectioncurve and ultimate load. This inconsistency can also be related to the failure mode. As shown in Fig. 3, the Sample 1 and 3 failed similarly, whereas the Sample 2 failed due to the misalignment of the beams. As a result, Sample 2 could not reach the full capacity resulting in 30 and 14% lower ultimate load carrying capacity compared to the same of Sample 1 and 3, respectively.

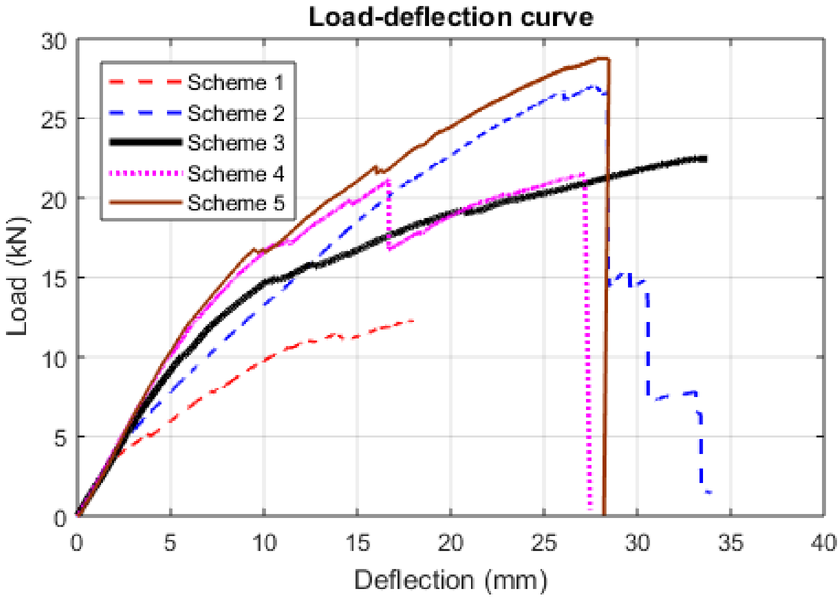

Fig. 6 Comparison among the load-deflection curve of the proposed 5 strengthening techniques under negative moment

Table 1 Failure mode and ultimate load of the proposed five strengthening schemes

		Ultimate load (kN)			
Scheme	Failure mode	S1	S2	S3	Mean
Scheme 1	CFRP fracture	12.4	10.4	9.4	10.7
Scheme 2	CFRP fracture	27.1	19.1	22.2	22.8
Scheme 3	Delamination of bi-directional CFRP	22.5	-	-	22.5
Scheme 4	Delamination of bi-directional CFRP	18.7	19.7	21.5	20.0
Scheme 5	Delamination of bi-directional CFRP	28.8	27.7	26.4	27.6

From the table, it is evident that the bi-direction CFRP alone can contribute significantly in terms of moment carrying capacity of the connection system. Fig. 6 compares the load-deflection curve of Scheme 3 against the same of other four schemes associated with the highest ultimate load of the corresponding scheme. The theoretical approach to predict the moment capacity for these five Schemes is discussed in the next section.

3. Theoretical models

Theoretical models for CFRP-LVL composite beam under positive moment was proposed by the authors in (Subhani *et al.* 2017). In this work, two models were compared – i) elastic-plastic model and ii) non-linear model. It was concluded that non-linear model is easier to implement and yield slightly better accuracy in terms of predicting ultimate moment capacity. Therefore, non-linear model is considered in this study as well.

For negative moment capacity, the tensile capacity of timber is ignored, since only CFRP is carrying tension at the connection system by providing continuity to the beams. Nevertheless, timber is carrying the compression at the joint. All other assumptions as described in (Subhani *et al.* 2017) related to non-linear model for the positive moment models remain same for negative moment prediction.

3.1 Scheme 1: Uni-directional CFRP strip

As described in Section 2, the beams related to this scheme were failed by CFRP fracture. Therefore, the failure strain is the fracture strain of CFRP strip. The section equilibrium along with stress-strain relationship of timber under compression is shown in Fig. 7.

The compressive force of the timber is as follows (Subhani *et al.* 2017)

$$F_c = f_{cu} b_t r_1 y_c^2 \left(1 - \frac{y_c r_1}{3}\right) \tag{1a}$$

$$r_1 = \frac{\varepsilon_{fu}}{y_f \varepsilon_{cu}} \tag{1b}$$

$$y_c = h + \frac{t_f}{2} - y_f \tag{1c}$$

where, F_c = compressive for in timber, f_{cu} = ultimate compressive strength of LVL, b_t = width of timber beam, y_c = distance between neutral axis and the compression face of the connection, ε_{fu} = ultimate tensile strain of CFRP, y_f = distance between neutral axis and the centroid of the CFRP, ε_{cu} = compressive strain of LVL beam related to ultimate strength, h = height of the LVL cross-section and t_f = thickness of CFRP.

The tensile forces carried by the CFRP on the ultimate tension face (F_{fs}) is

$$F_{fs} = E_f \varepsilon_{fu} b_f t_f \tag{2}$$

where, E_f = modulus of elasticity of CFRP and b_f = width of CFRP.

Therefore, the location of neutral axis (y_f) can be determined from force equilibrium

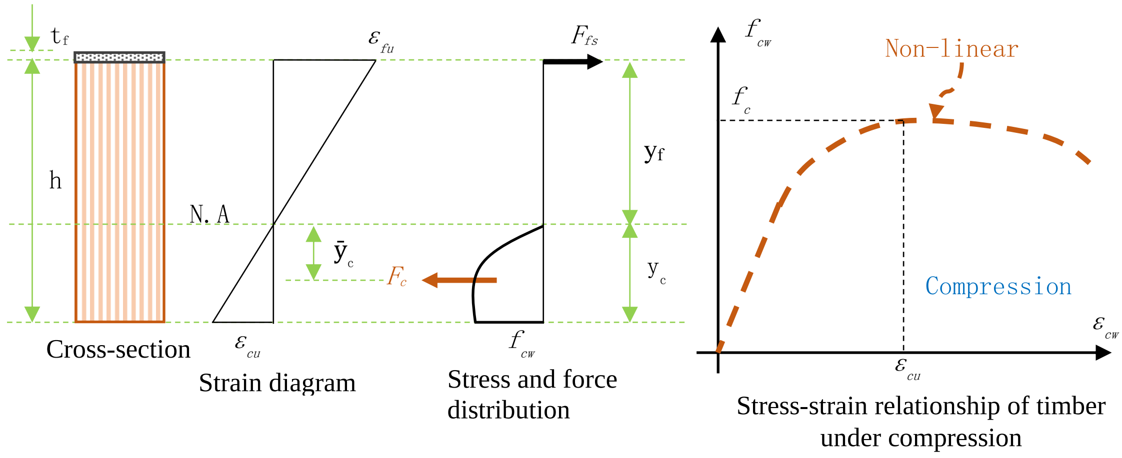

Fig. 7 Section equilibrium (Scheme 1)

$$F_c - F_{fs} = 0 \tag{3}$$

Finally, the ultimate moment capacity (M_u) of the section is given by

$$M_u = F_c \bar{y}_c + F_{fs} y_f \tag{4a}$$

$$\bar{y}_c = \frac{y_c\,(8 - 3y_c r_1)}{4\,(3 - y_c r_1)} \tag{4b}$$

where, $\bar{y}_c$ is the distance between centroid of the compressive force and the neutral axis (Subhani *et al.* 2017).

3.2 Scheme 2: Uni-directional CFRP U-wrap

Similar to Scheme 1, the beams related to this group also failed due to the CFRP fracture. For this scheme, the CFRP leg on the side of the cross-section of the beam will also participate in force resistance and contributes to the equilibrium and compatibility requirements at the cross section. However, the end segments of the CFRP U-wrap (CFRP leg) will act partially due to the free end constraints. This was also evident from the test observations and measurements as shown in Fig. 3. It has been observed that only 75% of the CFRP leg will be effective and hence considered in the equilibrium and compatibility check. This can be considered as the effective depth ($h_{f.eff}$) of the CFRP sheet on both sides of the cross section

$$h_{f.eff} = 0.75 h_{fu} \tag{5}$$

where, h_{fu} = height of the CFRP leg of the U-wrap.

Accordingly, two situation should be taken into consideration while determining moment carrying capacity of the section - Case a: when $y_f \le h_{f.eff}$ and Case b: when $y_f > h_{f.eff}$ (Fig. 8).

Therefore, the force acting on the CFRP legs (F_{fl}) is as follows

$$F_{fl} = \begin{cases} \dfrac{1}{2} E_f \varepsilon_{fu} y_f (2t_f), & y_f \le h_{f.eff} \\ \dfrac{1}{2} E_f (\varepsilon_{fu} + \varepsilon_{fm}) h_{f.eff} (2t_f), & y_f > h_{f.eff} \end{cases} \tag{6a}$$

$$\varepsilon_{fm} = \frac{\varepsilon_{fu}}{y_f}(y_f - h_{f.eff}) \tag{6b}$$

where, ε_{fm} = strain at the depth of $h_{f.eff}$ when $y_f > h_{f.eff}$.

Therefore, the force equilibrium to locate the neutral axis (y_f) is given by

$$F_c - F_{fs} - F_{fl} = 0 \tag{7}$$

Finally, the ultimate moment capacity of the cross-section is

$$M_u = \begin{cases} F_c \bar{y}_c + F_{fs} y_f + F_{fl}\left(\dfrac{2}{3} y_f\right), & y_f \le h_{f.eff} \\ F_c \bar{y}_c + F_{fs} y_f + F_{fl} \bar{y}_{fl}, & y_f > h_{f.eff} \end{cases} \tag{8a}$$

$$\bar{y}_{fl} = y_f - h_{f.eff} \frac{(2\varepsilon_{fm} + \varepsilon_{fu})}{3(\varepsilon_{fm} + \varepsilon_{fu})} \tag{8b}$$

where, $\bar{y}_{fl}$ = distance between the centroid of the F_{fl} and neutral when $y_f > h_{f.eff}$.

3.3 Scheme 3: Bi-directional CFRP wrap

The failure of the beam started due to the debonding of the bi-directional CFRP from the grain face of the LVL beam. It was previously investigated by the authors that the bond between LVL and CFRP is affected by the grain orientation of CFRP and LVL and also depends on which surface (grain or laminate face of LVL) the CFRP is attached (Subhani *et al.* 2017). The bond strength of CFRP to timber interface is described as (Juvandes and Barbosa 2012)

$$P_b = \begin{cases} P_u, & L_{eff} > L_b \\ P_{max}, & L_{eff} \le L_b \end{cases} \tag{9a}$$

$$P_u = P_{max} \frac{L_b}{L_{eff}}\left(2 - \frac{L_b}{L_{eff}}\right) \tag{9b}$$

$$P_{max} = c_1 k_b k_c K_\mu b_{fb} \sqrt{E_{fb} t_{fb} \tau_f} \tag{9c}$$

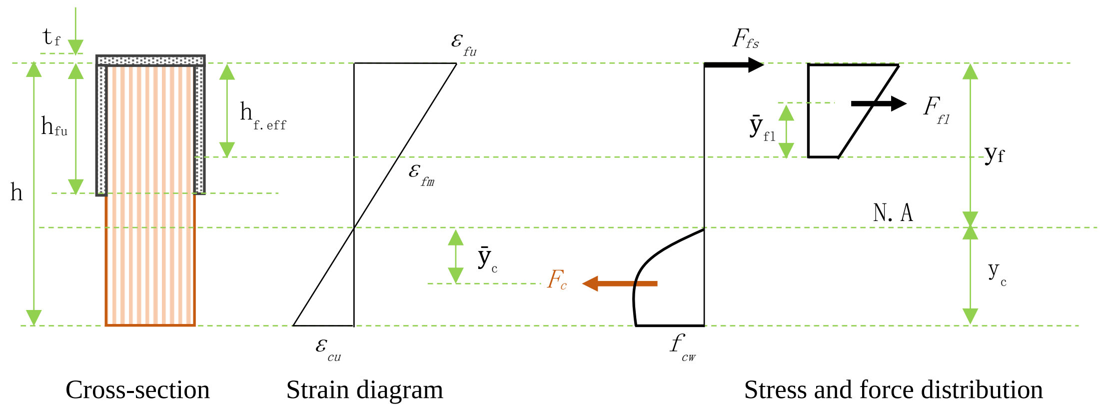

Fig. 8 Section equilibrium when $y_f > h_{f.eff}$ (Scheme 2)

$$L_{eff} = \sqrt{\frac{E_{fb} t_{fb}}{c_2 \tau_f}} \tag{9d}$$

$$k_b = 1.06 \sqrt{\frac{2 - \frac{b_{fb}}{b_{tb}}}{1 + \frac{b_{fb}}{400}}}, 1 \leq k_b \leq 1.29 \tag{9e}$$

where, L_b = bond length, L_{eff} = effective bond length, E_{fb}, b_{fb} = modulus of elasticity and width of the bi-directional CFRP, respectively, t_{fb} = thickness of one layer of bi-directional CFRP, τ_f = maximum shear stress along the bond length, b_{tb} = width of timber related to bi-directional CFRP, c_1 and c_2 = parameters obtained by experimental calibration, k_b = parameter affected by anchor zone geometry, k_c = parameter due to surface preparation effect and K_μ = strengthening degree. For the bi-directional wrap, $b_{fb} = b_{tb} = y_f$.

Determination of bond strength considering all the aforementioned parameters in Equation (9), grain / laminate face of LVL and fibre orientation difference between CFRP and LVL is discussed in detail in (Subhani *et al.* 2017). A brief overview will also be provided in Section 4. The ultimate debonding force is transferred to the bi-directional CFRP. As a result, the debonding strain (ε_{fb}) of bi-directional CFRP is

$$\varepsilon_{fb} = \frac{P_b}{E_{fb} t_{fb} b_{fb}} \leq \varepsilon_{fub} = \frac{f_{fub}}{E_{fb}} \tag{10}$$

where, ε_{fub} = ultimate strain of bi-directional CFRP and f_{fub} = ultimate tensile strength of bi-directional CFRP.

Accordingly, the tensile force carried out by the bi-directional CFRP wrap ($F_{fl.b}$) is given by

$$F_{fl.b} = \frac{1}{2} E_{fb} \varepsilon_{fb} y_f (4 t_{fb}) \tag{11}$$

Since bi-directional CFRP has two layers and attached on both sides connection, the thickness is multiplied by 4. The compressive force of the timber is as follows

$$F_c = f_{cu} b_t r_1 y_c^2 \left(1 - \frac{y_c r_1}{3}\right) \tag{12a}$$

$$r_1 = \frac{\varepsilon_{fb}}{y_f \varepsilon_{cu}} \tag{12b}$$

$$y_c = h - y_f \tag{12c}$$

Lastly, the location of neutral axis (y_f) and ultimate moment capacity can be determined as follows

$$F_c - F_{fl.b} = 0 \tag{13}$$

$$M_u = F_c \bar{y}_c + F_{fl.b} \left(\frac{2}{3} y_f\right) \tag{14}$$

3.4 Scheme 4: Combination of uni-directional CFRP strip and joint wrap using bi-directional CFRP

The failure mode observed for this group was also initiated by the delamination of the bi-directional CFRP. Consequently, Section 3.3 should be used with an additional force carried out by the uni-directional CFRP. Since failure strain for this scheme is related to the bi-directional CFRP, the tensile force acting on the uni-directional CFRP is given by

$$F_{fs} = E_f \varepsilon_{fb} b_f t_f \tag{15}$$

Finally, the force and moment equilibrium are given as

$$F_c - F_{fs} - F_{fl.b} = 0 \tag{16}$$

$$M_u = F_c \bar{y}_c + F_{fs} y_f + F_{fl.b} \left(\frac{2}{3} y_f\right) \tag{17}$$

3.5 Scheme 5: Combination of uni-directional CFRP U-wrap and joint wrap using bi-directional CFRP

This scheme also exhibit same failure mode as Scheme 3 and 4. As a result, delamination strain will govern. Therefore, Equations 9 – 12 and 15 are also applicable for

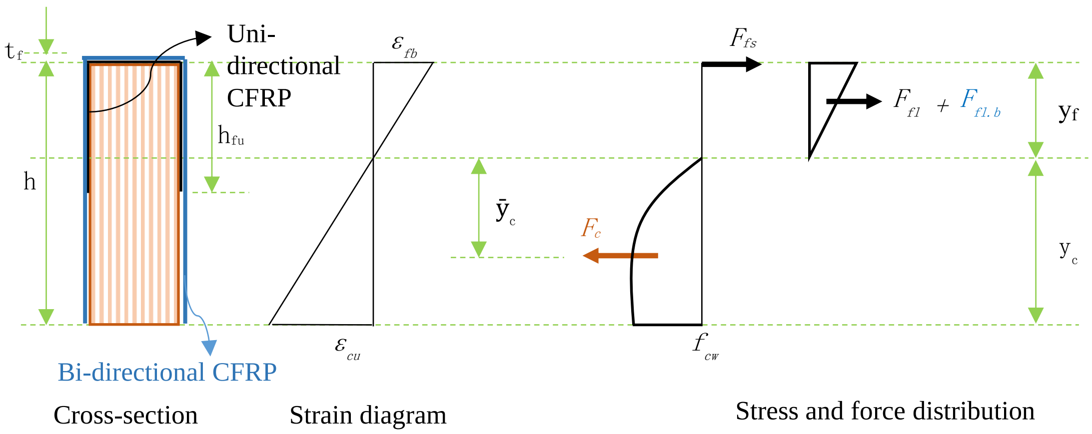

(a) when $y_f \leq h_{fu}$

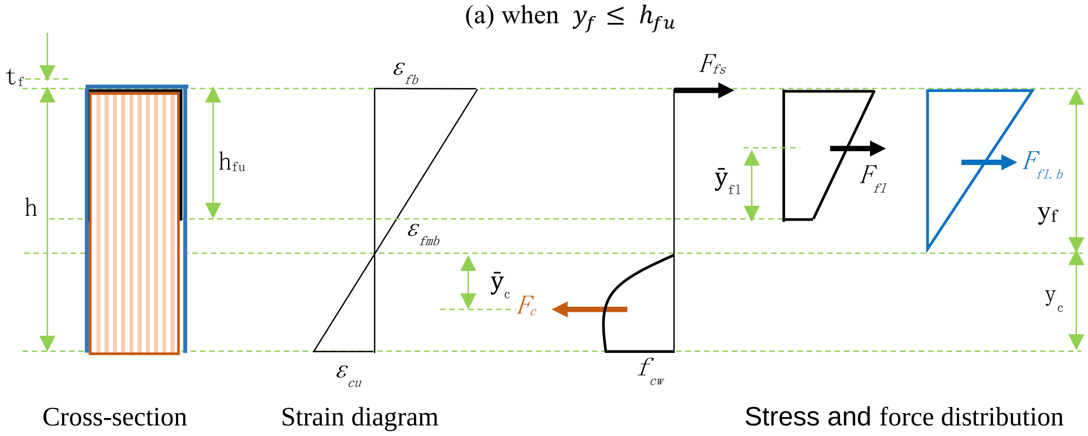

(b) when $y_f > h_{fu}$

Fig. 9 Section equilibrium for Scheme 5

Scheme 5. In addition, the CFRP leg of the U-wrap will also contribute to the force equilibrium. However, unlike Scheme 2, the full height of the CFRP leg will be active, since the bi-directional CFRP is providing sufficient anchorage to the uni-directional U-wrap.

Therefore, the force acting on the uni-directional CFRP legs (F_{fl}) yields

$$F_{fl} = \begin{cases} \frac{1}{2} E_f \varepsilon_{fb} y_f (2t_f), & y_f \leq h_{fu} \\ \frac{1}{2} E_f (\varepsilon_{fb} + \varepsilon_{fmb}) h_{fu} (2t_f), & y_f > h_{fu} \end{cases} \quad (18a)$$

$$\varepsilon_{fmb} = \frac{\varepsilon_{fb}}{y_f}(y_f - h_{fu}) \quad (18b)$$

where, ε_{fmb} = strain at the depth of h_{fu} when $y_f > h_{fu}$.

Therefore, the force equilibrium to locate the neutral axis (y_f) is given by

$$F_c - F_{fs} - F_{fl} - F_{fl.b} = 0 \quad (19)$$

Finally, the ultimate moment capacity of the cross-section for Scheme 5 is as follows

$$M_u = \begin{cases} F_c \bar{y}_c + F_{fs} y_f + (F_{fl} + F_{fl.b}) \left(\frac{2}{3} y_f\right), y_f \leq h_{fu} \\ F_c \bar{y}_c + F_{fs} y_f + F_{fl} \bar{y}_{fl} + F_{fl.b} \left(\frac{2}{3} y_f\right), y_f > h_{fu} \end{cases} \quad (20a)$$

$$\bar{y}_{fl} = y_f - h_{fu} \frac{(2\varepsilon_{fmb} + \varepsilon_{fb})}{3(\varepsilon_{fmb} + \varepsilon_{fb})} \quad (20b)$$

where, $\bar{y}_{fl}$ = distance between the centroid of the F_{fl} and neutral axis when $y_f > h_{fu}$.

4. Validation of theoretical models

To validate the proposed theoretical model, the same material properties from the previous works (Subhani *et al.* 2017, Subhani *et al.* 2017, Globa *et al.* 2018) are used. As a result, the values associated with the parameters described in Section 3 are: f_{cu} = 47 MPa, ε_{cu} = 0.006, ε_{fu} = 0.0147, E_f = 216,000 MPa, f_{fu} = 3176 MPa, E_{fb} = 235,000 MPa, f_{fub} = 3500 MPa, b_t = 45 mm, b_f = 45 mm, h = 240 mm, h_{fu} = 115 mm, t_f = 0.131 mm, t_{fb} = 0.225 mm and L_b (bi-directional CFRP) = 240 mm.

To determine the parameters related to the bond properties (Equation 9(c) and (d)), the grain orientation of LVL and CFRP should be taken into account. In the previous work (Subhani *et al.* 2017), the authors considered three conditions which affect the bond strength. These were – i) CFRP applied parallel to the grain direction of LVL but attached on the laminate face of LVL, ii) CFRP applied parallel to the grain direction of LVL but attached on the

Table 2 Predicted moment capacity of the beams using the proposed theoretical models

Strengthening scheme	Exp. moment (kN.m)			Theoretical moment (kN.m)	Ratio (exp./theo.)		
	Sample 1	Sample 2	Sample 3		Sample 1	Sample 2	Sample 3
Scheme 1	5.58	4.68	4.23	4.31	**1.29**	**1.08**	**0.98**
Scheme 2	12.20	8.60	10.00	13.93	**0.88**	**0.62**	**0.72**
Scheme 3	10.12	-	-	9.34	**1.08**	-	-
Scheme 4	8.42	8.86	9.67	10.17	**0.83**	**0.87**	**0.95**
Scheme 5	12.96	12.47	11.88	12.53	**1.03**	**0.99**	**0.95**

grain face of LVL and iii) CFRP applied perpendicular to the grain direction of LVL but attached on the laminate face of LVL. In the proposed strengthening schemes (Scheme 3 – 5), the bi-directional CFRP was attached on the grain face of the LVL. Therefore, c_1, k_c and K_μ should be taken as 0.7, 0.75 and 1.0, respectively (Subhani *et al*. 2017). On the contrary, the angle between the fibre orientation of CFRP and LVL is 45°. Consequently, resultant values of c_2 and τ_f are considered for the 45° angle.

The values of c_2 were proposed as 10.0 and 3.0 when CFRP is applied parallel (0°) and perpendicular (90°) to the grain orientation of the LVL, respectively (Subhani *et al*. 2017). In addition, the maximum shear stress along the bond length (τ_f) was determined as 1.954 and 1.683 when CFRP is applied parallel (0°) and perpendicular (90°) to the grain orientation of the LVL, respectively (Subhani *et al*. 2017). As a result, the resultant of c_2 and τ_f for 45° angle between CFRP and LVL are calculated as 10.44 and 2.579, respectively.

Using the material and geometrical properties described above, the theoretical moment capacity for the proposed five schemes is determined and compared against the experimental moment capacity. Table 2 compares the theoretical vs experimental moment capacity of all three samples associated with various schemes. From the table, it is evident that the proposed theoretical models can predict the moment with satisfactory precision. It can be noted here though that the accuracy of the theoretical model for Scheme 2 shows large variation. This can be attributed to the explanation provided in Section 2. As illustrated in Fig. 5(b), large variations among the three samples in terms of ultimate load carrying capacity can be observed. Since Sample 1 was failed due to CFRP fracture, the LVL-CFRP composite beam reached its ultimate capacity and hence, the theoretical prediction yields satisfactory accuracy. In contrast, the Sample 2 of Scheme 2 failed due to misalignment of the beams resulted in premature failure of the composite beam (Fig. 3). As a result, poor prediction is obvious. The Sample 3 of this scheme was failed due the combined action of CFRP fracture and misalignment of the beams.

It can be concluded that even though the Scheme 2 improve the moment capacity by 300% compared to Scheme 1, the inconsistency in ultimate load carrying capacity can be expected due to the misalignment of the connected members which affect the performance to a great deal. This can be improved or eliminated by providing confinement using bi-directional CFRP wrap (Scheme 5).

As shown in Table 2, even though Scheme 5 has a 10% reduction in ultimate moment capacity (theoretical) compared to Scheme 2, it exhibits more consistent result in terms of ultimate moment capacity. Lastly, it can be noted that use of bi-directional CFRP only (Scheme 3) can enhance the moment capacity by 215% while comparing against Scheme 1.

5. Comparison among strengthening schemes

Moment-rotation behavior is commonly used to determine the efficacy of a connection system. Previous research reported the moment-rotation behavior of tenon and mortise connection (Xue *et al*. 2018) and fasteners (Allotey and Foschi 2005). In this section, the moment-rotation behaviour of the proposed five schemes will be compared. In addition, the moment-rotation behaviour subjected to positive moment will also be taken into account. For the positive moment testing, two strengthening schemes were proposed, as shown in Fig. 10. The two schemes are denoted as FS (CFRP strip) and UW (CFRP U-wrap). The theoretical model for positive moment was described in (Subhani *et al*. 2017).

To determine the moment-rotation behaviour, the proposed theoretical models is used. This is an iterative process for which the strain values are increased incrementally till the failure strain. In each step, the location of neutral axis can be determined and hence, the curvature or rotation using the following equations

$$\varepsilon_{c.i=1:n} = \frac{\varepsilon_{f.i=1:n} y_{c.i=1:n}}{y_{f.i=1:n}} \tag{21a}$$

$$\theta_{i=1:n} = \frac{\varepsilon_{c.i=1:n}}{y_{c.i=1:n}} \tag{21b}$$

where, $\varepsilon_{f.i=1:n}$ = strain value at ith step where n is associated with the failure strain corresponding to a particular scheme, $y_{f.i=1:n}$ = location of neutral axis from the furthest tension fibre for ith strain value, $y_{c.i=1:n}$ = location of neutral axis from the furthest compression fibre for ith strain value and $\theta_{i=1:n}$ = curvature at ith strain value.

The theoretical moment at each step can also be determined and therefore, the moment vs rotation curve for each strengthening scheme can be plotted, as depicted in Fig. 11. Three types of failure strain were observed for these

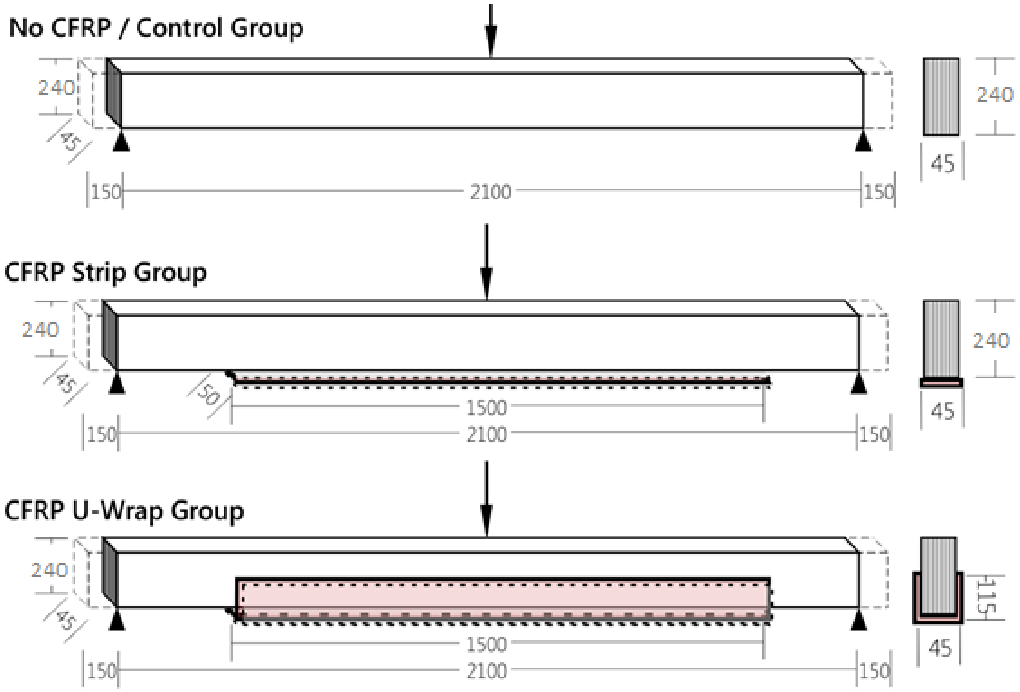

Fig. 10 Experimental program for LVL-CFRP composite beams under positive moment (Subhani *et al*. 2017)

schemes. The control, FS and UW groups failed due to the tensile failure of the LVL, whereas Scheme 1 and 2 failed due to CFRP fracture, and the failure for Scheme 3-5 were initiated by the debonding of bi-directional CFRP. As a result, the failure strain for Scheme 1 and 2 is 0.0147, for Scheme 3-5 is 0.0037 and for the positive moment, the failure strain is 0.0044.

Fig. 11 compares the moment-rotation behaviour of the beams subjected to negative moment against the beams subjected to positive moment. Even though the moment-rotation behaviour of beams subjected to positive moment not necessarily represent a rigid connection, it can be used as a benchmark to compare the performance of the Scheme 1-5. The moment-rotation characteristic of beams subjected to negative moment exhibits linear behaviour compared to the positive moment ones. This is obvious due to the fact that the moment-rotation characteristics of the control, FS and UW beams are governed by the timber properties which is non-linear. On the contrary, CFRP behaves linearly elastic till failure which is the failure mode for Scheme 1 and 2. Even though the debonding behaviour is non-linear (Biscaia *et al*. 2016, Biscaia *et al*. 2017, Subhani *et al*. 2017), it behaves linearly till the maximum debonding strength of the LVL-to-CFRP interface which governs the debonding strain for Scheme 3v5.

Table 3 Rotational rigidity of various strengthening schemes

Test type	Scheme	R_j (kN.m^2)	Ratio
Positive moment	Control	798.95	1.00
	FS	806.50	1.01
	UW	806.50	1.01
Negative moment	Scheme 1	61.80	0.08
	Scheme 2	171.47	0.21
	Scheme 3	386.10	0.48
	Scheme 4	414.03	0.52
	Scheme 5	466.34	0.58

The slope of the moment-rotation curve is denoted as rotational rigidity, R_j. For the negative moment, determination of rotation rigidity is straightforward due to the linear behaviour of the moment-rotation curve. For the positive moment, however, the moment-rotation curve can be simplified and represent as a tri-linear curve, denoted by points 0, 1, 2 and 3 in Fig. 12. Accordingly, the slope of the line connecting the points 0 and 2 is considered as the rotation rigidity for the control, FS and UW beams. Table 3 lists the rotational rigidity of all the beams. It is evident from the table that the rigidity increases from Scheme 1 to 5, and Scheme 5 attain the maximum rotational rigidity among the beams subjected to negative moment. In addition, the rotational rigidity significantly increases with the use of bi-directional CFRP. While comparing against the control beam under positive moment, Scheme 5 gained almost 58% of the rigidity.

It can be concluded that the implementation of uni-directional and bi-directional CFRP can effectively transfer the moment from one beam element to another. It is worthwhile to mention here that only one layer of uni and bi-directional CFRP were used in this study. By increasing thickness of CFRP, rotational rigidity can potentially be increased even further.

6. Conclusions

In this study, comparison among different strengthening schemes are considered to investigate the negative moment

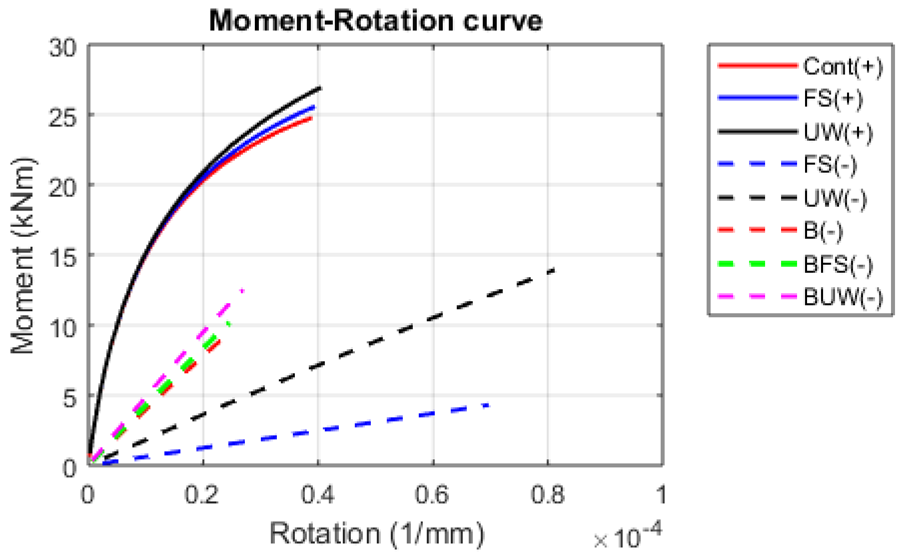

Fig. 11 Moment-rotation curve of the LVL-CFRP composite beams under positive and negative moment

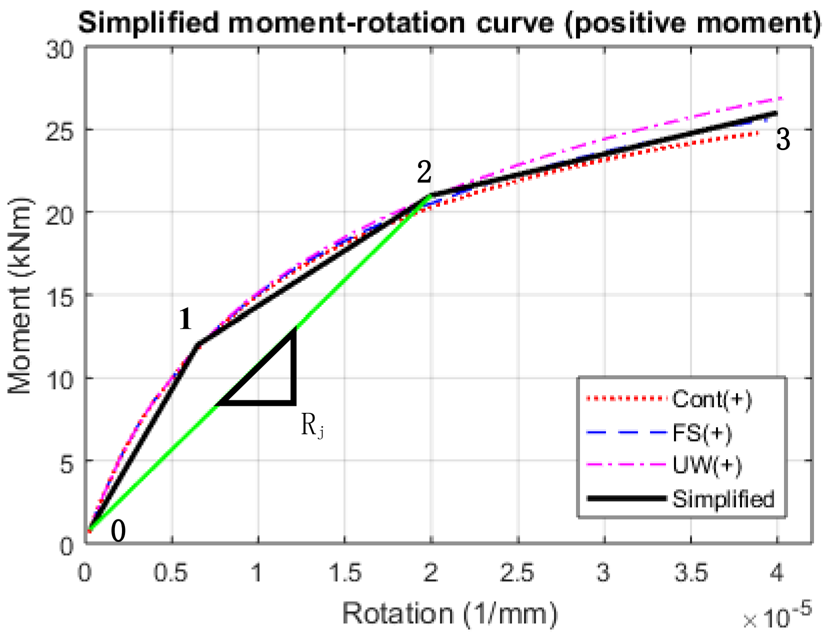

Fig.12 Rotational rigidity calculation for positive moment

carrying capacity of LVL-CFRP composite beams. Theseschemes provide continuity of the beams over a joint by using i) uni-directional CFRP strip, ii) uni-directional CFRP U-wrap, iii) bi-directional CFRP U-wrap, iv) bi-directional CFRP U-wrap + uni-directional CFRP strip and v) bi-directional CFRP U-wrap + uni-directional CFRP U-wrap. Two types of failure modes were observed for these strengthening techniques – CFRP fracture and delamination of bi-directional CFRP. It is found that the implementation of bi-directional CFRP is not only beneficial for increasing the moment capacity at the joint, but also to obtain consistent results.

Theoretical models are proposed to predict the theoretical moment capacity of the schemes by considering the appropriate failure mode. At the joint, timber is carrying compression and CFRP is solely carrying the tension. LVL beam is considered to behave non-linearly under compression, while CFRP is considered to behave elastic till failure. The proposed model can predict the experimental moment capacities to a satisfactory accuracy. It is found that uni-directional U-wrap has the highest moment carrying capacity, since these beams failed due to CFRP fracture. However, as observed in the experiments, the slight misalignment of the beams may cause premature failure of these beams. Implementation of bi-directional CFRP along with the uni-directional U-wrap provide more consistent result with a decrease of only 10% moment carrying capacity. The failure mode also shift to debonding of bi-directional CFRP rather than CFRP fracture or misalignment of the connected beams.

The validated theoretical model is also used to plot the moment-rotation behaviour of the proposed strengthening schemes and compared against the control and LVL-CFRP composite beams subjected to positive moment. For the positive moment, LVL beam with CFRP strip and CFRP U-wrap are taken into account. The moment-rotation behaviour for the negative moment is found to be linear, since both the failure modes (CFRP fracture and delamination of FRP) exhibit liniear behaviour till the ultimate moment capacity. For the positive moment, the moment-rotation relationship is governed by the properties of timber and found to be non-linear.

The rotational rigidity of all the beams subjected to positive and negative moments is determined from the moment-rotation curve and compared. It is observed that the Scheme 5 has the highest rotational rigidity while comparing against the other schemes subjected to negative moment. In relation to the control beam, the Scheme 5 gain 58% of the rotation rigidity of an LVL beam under positive moment. It can be noted here that only one layer of bi- and uni-directional CFRP are used in Scheme 5 and higher rotational rigidity and moment capacity can be expected for thicker CFRPs. As a result, it can be concluded that the LVL-CFRP composite beams with bi- and uni-directional CFRP U-wrap has satisfactory capacity in terms of both moment carrying capacity and rotational rigidity.

Acknowledgments

This project is funded by Faculty of Science, Engineering and Built Environment of Deakin University under the Industry Engagement Scheme. The authors express their gratitude to the industry partner Arup for their involvement and in-kind support. Also, the authors would like to thank Mr Lube Veljanoski and Dr Muhammad Ikramul Kabir for their support in this project.

References

Alhayek, H. and Svecova, D. (2012), "Flexural stiffness and strength of GFRP-reinforced timber beams", *J. Compos. Construct.*, **16**(3), 245-252. https://doi.org/10.1061/(ASCE)CC.1943-5614.0000261

Allotey, N. and Foschi, R. (2005), "Frictional effects on the cyclic response of laterally loaded timber fasteners", *Struct. Eng. Mech.*, **21**(1), 1-18. https://doi.org/10.12989/sem.2005.21.1.001

Biscaia, H.C., Chastre, C., Cruz, D. and Franco, N. (2016), "Flexural Strengthening of Old Timber Floors with Laminated Carbon Fiber–Reinforced Polymers", *J. Compos. Construct.*, **21**(1). https://doi.org/10.1061/(ASCE)CC.1943-5614.0000731.

Biscaia, H.C., Chastre, C., Cruz, D. and Viegas, A. (2017), "Prediction of the interfacial performance of CFRP laminates and old timber bonded joints with different strengthening techniques", *Compos. Part B Eng.*, **108**, 1-17. https://doi.org/10.1016/j.compositesb.2016.09.097

Biscaia, H.C., Cruz, D. and Chastre, C. (2016), "Analysis of the debonding process of CFRP-to-timber interfaces", *Consruct. Build. Mater.*, **113**, 96-112. https://doi.org/10.1016/j.conbuildmat.2016.03.033

Chun, Q., Balen, K.V. and Pan, J. (2016), "Flexural Performance of Small Fir and Pine Timber Beams Strengthened With Near-Surface Mounted Carbon-Fiber-Reinforced Polymer (NSM CFRP) Plates and Rods", *J. Architect. Heritage*, **10**(1), 106-117. https://doi.org/10.1080/15583058.2014.971195

D'Ambrisi, A., Focacci, F. and Luciano, R. (2014), "Experimental investigation on flexural behavior of timber beams repaired with CFRP plates", *Compos. Struct.*, **108**, 720-728. https://doi.org/10.1016/j.compstruct.2013.10.005

De la Rosa García, P., Escamilla, A.C. and García, M.N.G. (2013), "Bending reinforcement of timber beams with composite carbon fiber and basalt fiber materials", *Compos. Part B Eng.*, **55**, 528-536. https://doi.org/10.1016/j.compositesb.2013.07.016

De la Rosa García, P., Escamilla, A.C. and García, M.N.G. (2016), "Analysis of the flexural stiffness of timber beams reinforced with carbon and basalt composite materials", *Compos. Part B Eng.*, **86**, 152-159. https://doi.org/10.1016/j.compositesb.2015.10.003

De Lorenzis, L., Scialpi, V. and La Tegola, A. (2005), "Analytical and experimental study on bonded-in CFRP bars in glulam timber", *Compos. Part B Eng.*, **36**(4), 279-289. https://doi.org/10.1016/j.compositesb.2004.11.005

Fiorelli, J. and Dias, A.A. (2003), "Analysis of the strength and stiffness of timber beams reinforced with carbon fiber and glass fiber", *Mater. Res.*, **6**(2), 193-202. http://dx.doi.org/10.1590/S1516-14392003000200014

Fossetti, M., Minafò, G. and Papia, M. (2015), "Flexural behaviour of glulam timber beams reinforced with FRP cords", *Consruct. Build. Mater.*, **95**, 54-64. https://doi.org/10.1016/j.conbuildmat.2015.07.116

Globa, A., Subhani, M., Moloney, J. and Al-Ameri, R. (2018), "Carbon Fiber and Structural Timber Composites for Engineering and Construction", *J. Architect. Eng.*, **24**(3). https://doi.org/10.1061/(ASCE)AE.1943-5568.0000318.

Guan, Z. and Rodd, P. (2003), "Modelling of timber joints made with steel dowels and locally reinforced by DVW discs", *Struct. Eng. Mech.*, **16**(4), 391-404. https://doi.org/10.12989/sem.2003.16.4.391

Juvandes, L. and Barbosa, R. (2012), "Bond Analysis of Timber Structures Strengthened with FRP Systems", *Strain*, **48**(2), 124-135. https://doi.org/10.1111/j.1475-1305.2011.00804.x

Khelifa, M., Auchet, S., Méausoone, P.J. and Celzard, A. (2015), "Finite element analysis of flexural strengthening of timber beams with Carbon Fibre-Reinforced Polymers", *Eng. Struct.*, **101**, 364-375. https://doi.org/10.1016/j.engstruct.2015.07.046

Khelifa, M. and Celzard, A. (2014), "Numerical analysis of flexural strengthening of timber beams reinforced with CFRP strips", *Compos. Struct.*, **111**, 393-400. https://doi.org/10.1016/j.compstruct.2014.01.011

Khelifa, M., Lahouar, M.A. and Celzard, A. (2015), "Flexural strengthening of finger-jointed Spruce timber beams with CFRP", *J. Adhesion Sci. Technol.*, **29**(19), 2104-2116. https://doi.org/10.1080/01694243.2015.1057395

Li, Y.-F., Xie, Y.-M. and Tsai, M.-J. (2009), "Enhancement of the flexural performance of retrofitted wood beams using CFRP composite sheets", *Consruct. Build. Mater.*, **23**(1), 411-422. https://doi.org/10.1016/j.conbuildmat.2007.11.005

Micelli, F., Scialpi, V. and La Tegola, A. (2005), "Flexural reinforcement of glulam timber beams and joints with carbon fiber-reinforced polymer rods", *J. Compos. Construct.*, **9**(4), 337-347. https://doi.org/10.1061/(ASCE)1090-0268(2005)9:4(337)

Miljanovic, S. and Zlatar, M. (2015), "Theoretical and experimental research of external prestressed timber beams in variable moisture conditions", *Coupled Syst. Mech.*, **4**(2), 191-209. https://doi.org/10.12989/csm.2015.4.2.191

Nowak, T.P., Jasieńko, J. and Czepiżak, D. (2013), "Experimental tests and numerical analysis of historic bent timber elements reinforced with CFRP strips", *Consruct. Build. Mater.*, **40**, 197-206. https://doi.org/10.1016/j.conbuildmat.2012.09.106

Raftery, G.M. and Harte, A.M. (2011), "Low-grade glued laminated timber reinforced with FRP plate", *Compos. Part B Eng.*, **42**(4), 724-735. https://doi.org/10.1016/j.compositesb.2011.01.029

Schober, K.-U., Harte, A.M., Kliger, R., Jockwer, R., Xu, Q. and Chen, J.-F. (2015), "FRP reinforcement of timber structures", *Consruct. Build. Mater.*, **97**, 106-118. https://doi.org/10.1016/j.conbuildmat.2015.06.020

Schober, K. and Rautenstrauch, K. (2005). "Experimental investigation on flexural strengthening of timber structures with CFRP", *Proceedings of the International Symposium on Bond Behavior of FRP in Structures*, Hong Kong, December.

Smith, S.T. (2011), *Strengthening of concrete, metallic and timber construction materials with FRP composites*, Springer, Berlin, Germany.

Subhani, M., Globa, A., Al-Ameri, R. and Moloney, J. (2017), "Effect of grain orientation on the CFRP-to-LVL bond", *Compos. Part B Eng.*, **129**, 187-197. https://doi.org/10.1016/j.compositesb.2017.07.062

Subhani, M., Globa, A., Al-Ameri, R. and Moloney, J. (2017), "Flexural strengthening of LVL beam using CFRP", *Consruct. Build. Mater.*, **150**, 480-489. https://doi.org/10.1016/j.conbuildmat.2017.06.027

Wan, J., Smith, S.T. and Qiao, P. (2011), *FRP-to-softwood Joints: Experimental Investigation*, Springer, Berlin, Germany.

Xue, J., Qi, L., Dong, J. and Xu, D. (2018), "Analytical investigation on moment-rotation relationship of through-tenon joints with looseness in ancient timber buildings", *Earthq. Struct.*, **14**(3), 241-248. https://doi.org/10.12989/eas.2018.14.3.241

CC